Vortex structures in model p-wave superconducting Sr_2RuO_4: Single two-dimensional band vs quasi-one-dimensional bands

Jia-Wei Huo[1] and Fu-Chun Zhang[1,2]
[1]*Department of Physics, The University of Hong Kong, Hong Kong, China*
[2]*Department of Physics, Zhejiang University, Hangzhou 310027, China*
(Received 9 February 2013; revised manuscript received 25 March 2013; published 2 April 2013)

There has been an interesting debate on the primary source of chiral p-wave superconductivity in Sr_2RuO_4. We present a comparative study on the vortex structure between a single two-dimensional (2D) band and quasi-1D band model by using the Bogoliubov-de Gennes theory. The pattern of the local density of states at zero bias around a vortex core has a diamond shape in the quasi-1D model and is much more isotropic in the 2D model. The spin-lattice relaxation rate well below the superconducting transition temperature is greatly enhanced in the vortex state in the 2D model, but not in the quasi-1D model. These features can be tested by using a scanning tunneling microscope and nuclear magnetic resonance or nuclear quadrupole resonance to distinguish the models for the superconductivity in Sr_2RuO_4.

DOI: 10.1103/PhysRevB.87.134501 PACS number(s): 74.25.Ha, 74.70.Pq, 74.20.Mn

I. INTRODUCTION

The layered perovskite material Sr_2RuO_4 has attracted a lot of interest due to the experimental evidence for its spin-triplet superconductivity with broken time-reversal symmetry.[1] Shortly after the discovery of its superconductivity,[2] Rice and Sigrist[3] and Baskaran[4] pointed out that the superconducting state might be an electronic analog of the ^{3}He-A phase. Within this scenario, assuming the simplest nearest-neighbor pairing interaction, the gap function in terms of the d-vector formalism can be expressed compactly as[5,6]

$$\vec{d}(\boldsymbol{k}) = \Delta_0 \hat{z}(\sin k_x + i \sin k_y). \quad (1)$$

Sr_2RuO_4 is a quasi-two-dimensional (2D) system. Its normal state can be well described by a multiorbital band structure with a 2D γ band derived from the Ru d_{xy} orbital and two weakly hybridized quasi-1D α and β bands derived from Ru d_{xz} and d_{yz} orbitals (Fermi surfaces of this material will be shown below). Due to the distinct orbital character of different bands, a superconducting state with equal gaps in all three bands is unlikely. The orbital nature of superconductivity in Sr_2RuO_4 has been discussed on a very general basis,[7] which suggests that the superconducting pairing is predominantly derived from either the γ or the α and β bands, but superconductivity can be induced in the passive Fermi surfaces via a weak proximity effect. This picture is supported by the specific-heat measurement in a magnetic field.[8] In this experiment, the in-plane field dependence of the specific heat shows a "shoulder" structure at low fields, corresponding to about half of the total density of states in the normal phase. Combining this result with the information on the density of states of different bands from quantum oscillations,[9] the only consistent physical picture would be either the 2D γ band or the quasi-1D α and β bands as the active source of superconductivity below the transition temperature. Nevertheless, due to the weak proximity effect, all of the bands become gapped only at a temperature approaching zero. Therefore, in a wide temperature range well below the transition, it is still an unsolved issue as to which portion of Fermi surfaces is the active source of superconductivity.

It is natural and has been generally assumed that superconductivity arises primarily on the 2D γ band,[3] referred to as the 2D model hereafter. The directional variation of the specific-heat experiment in a magnetic field is slightly in favor of this scenario.[8] However, basic questions concerning the primary source of the pairing remain controversial due to important discrepancies between theory and experiment, in spite of intense research work in the past almost two decades.[10,11] For example, the 2D model predicts an edge current in the superconducting state due to robust Andreev bound states in the surface,[12,13] which has not been demonstrated,[14,15] although this also has been controversial.[11,16,17] Very recently, Raghu *et al*. suggested an alternative interesting possibility for the spin-triplet superconductivity in Sr_2RuO_4,[16,18] where the dominant superconducting instability in the triplet channel occurs on the quasi-1D α and β bands, hybridized from the Ru d_{xz} and d_{yz} orbitals. This model (quasi-1D model hereafter) predicts the absence of topologically protected edge modes, contrary to the single 2D band model. One also expects an intrinsic anomalous Hall effect due to the multiband nature of this model,[19,20] different from the single-band scenario,[21] which may explain the observation of the nonzero Kerr effect.[22] On the other hand, the quasi-1D model would predict a suppression of spin-density wave fluctuation at the superconducting transition point,[23] which has not been seen in neutron experiments thus far.[24] Therefore, it is important to explore the possibilities for more experimental consequences within the 2D band or quasi-1D band models and to test the model against experiments.

In the single 2D band picture, a Cooper pair in the chiral p-wave state is illustrated schematically in Fig. 1(a), while its counterpart in the two quasi-1D band picture is shown in Fig. 1(b). It is highly demanding to distinguish the two possibilities by using available experimental probes. However, the fragile superconducting state of Sr_2RuO_4 does pose a challenge and restriction to experimental probes. For example, the low transition temperature with $T_c \approx 1.5$ K is beyond the present technical limit using state-of-the-art angle-resolved photoemission spectroscopy.[25] In order to pin down this controversial issue with currently available experiments,

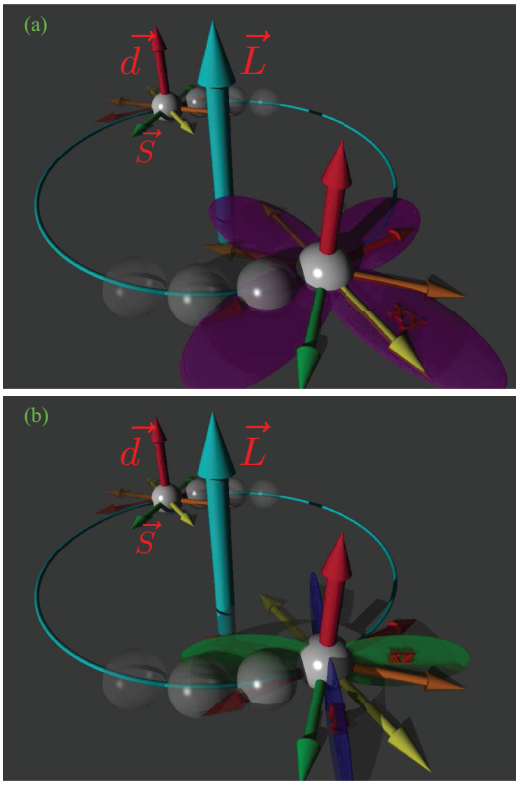

FIG. 1. (Color online) Schematic illustrations of a Cooper pair with spin $\vec{S}$ and orbital angular momentum $\vec{L}$ for a spin-triplet superconductor in the chiral state with $\vec{d}(\boldsymbol{k})$ formed in (a) the single band and (b) quasi-1D bands. In the former case, superconductivity is mainly from the d_{xy} orbital, whereas the hybridization of d_{xz} and d_{yz} orbitals play a key role in the latter case. It is strongly desirable to distinguish these two scenarios in order to identify the orbital origin of superconductivity.

in this work we study the vortex phase of a chiral p-wave superconductor for both the 2D band and quasi-1D band scenarios. It is found that different models give rise to qualitatively distinguishable vortex states, which is a promising characteristic to identify the underlying superconducting nature of Sr_2RuO_4.

The rest of this paper is organized as follows. In Sec. II, some basic properties of the Fermi surface in the normal state are studied. In Sec. III, we construct the effective Hamiltonians based on the Bogoliubov-de Gennes theory for two different models as a pedagogical procedure. In Sec. IV, the results with a focus on experimental observables are presented. We note that the vortex state for the single-band chiral p-wave model has been studied in previous literature.[26] In the present work, we use more realistic parameters for the purpose of direct comparison of two different models. Finally, a concluding remark is given in Sec. V.

II. PROPERTY OF NORMAL STATE: FERMI SURFACE

Before proceeding to the discussion of a different superconducting model, we briefly discuss the topology of the Fermi surface in the normal state. As we will see later, the Fermi surfaces of different bands give rise to different signatures corresponding to the superconducting states. We begin with the Hamiltonian in the $4d - t_{2g}$ orbital basis of the Ru ions,

$$\hat{H}_{\boldsymbol{k}} = \begin{pmatrix} \xi_1(\boldsymbol{k}) & g(\boldsymbol{k}) & 0 \\ g(\boldsymbol{k}) & \xi_2(\boldsymbol{k}) & 0 \\ 0 & 0 & \xi_3(\boldsymbol{k}) \end{pmatrix}, \tag{2}$$

where $\xi_1(\boldsymbol{k}) = -2t\cos k_x - \mu$, $\xi_2(\boldsymbol{k}) = -2t\cos k_y - \mu$, $g(\boldsymbol{k}) = -4t'\sin k_x \sin k_y$, and $\xi_3(\boldsymbol{k}) = -2t_3(\cos k_x + \cos k_y) - 4t_3'\cos k_x \cos k_y - \mu_3$. Here, 1, 2, and 3 denote orbitals xz, yz, and xy, respectively. Hereafter we take $(t,t',t_3,t_3') = (1,0.1,0.8,0.35)$ for the hopping parameters, and (μ,μ_3) are fine tuned such that the electron density for each band is equal to 4/3.[27] Note that this set of parameters can reproduce a Fermi surface, whose shape agrees with that obtained in the angle-resolved photoemission spectroscopy measurement above T_c.[28]

After diagonalizing the Hamiltonian in Eq. (2), the Fermi surface can be obtained, as shown in Fig. 2(a). It is noted that

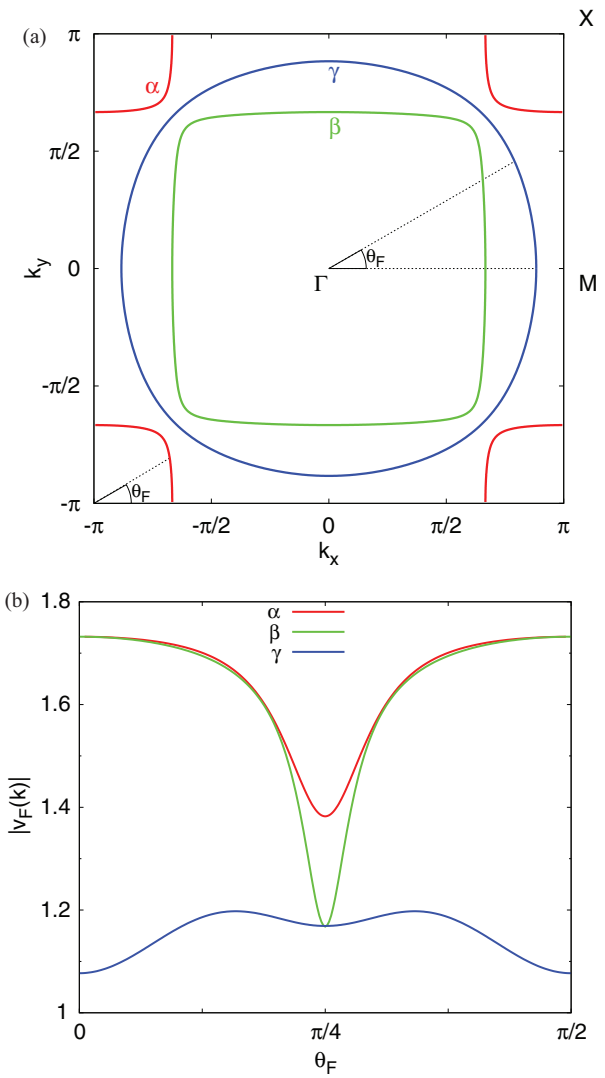

FIG. 2. (Color online) (a) Two-dimensional Fermi surface for Sr_2RuO_4 in the normal state. (b) Amplitude of Fermi velocity $v_F(\boldsymbol{k})$ along the Fermi-surface line. Here, θ_F is the angle between the point $\boldsymbol{k}$ on the Fermi surface and x axis, as indicated in the figure.

the γ band is almost isotropic in the two-dimensional plane, whereas the quasi-1D α,β bands show significant anisotropy. To further illustrate this point, we show the amplitude of Fermi velocity $\vec{v}_F(\boldsymbol{k})$ in different bands in Fig. 2(b). We can see that $|\vec{v}_F(\boldsymbol{k})|$ is maximized along the in-plane square lattice axis a or b for the α and β bands, while it is almost isotropic for the γ band.

In the subsequent sections related to the superconducting state, we will concentrate the discussion on the vortex state in order to provide a good test and to answer the question of which band superconductivity takes place in. As we will see later, the topology of the Fermi surface is actually inherited in the superconducting state for which the band is predominant.

III. BOGOLIUBOV-DE GENNES THEORY OF THE SUPERCONDUCTING STATE

A. Single 2D band model

First, we consider a single 2D band model based on the d_{xy} orbital. In terms of the eigenenergy E_ϵ and the quasiparticle amplitudes u_i^ϵ, v_i^ϵ at the ith site, the Bogoliubov-de Gennes equations are given by[26]

$$\sum_j \begin{bmatrix} H_{ij} & \Delta_{ij} \\ \Delta_{ij}^\dagger & -H_{ij}^* \end{bmatrix} \begin{bmatrix} u_j^\epsilon \\ v_j^\epsilon \end{bmatrix} = E_\epsilon \begin{bmatrix} u_i^\epsilon \\ v_i^\epsilon \end{bmatrix}, \tag{3}$$

where $H_{ij} = -t_{ij} e^{i\varphi_{ij}} - \mu_3 \delta_{i,j}$, and ϵ is an index of the eigenstate. The magnetic field is introduced through the Peierls phase factor $e^{i\varphi_{ij}}$ with $\varphi_{ij} = \frac{\pi}{\Phi_0}\int_{r_j}^{r_i} \mathbf{A}(\mathbf{r})\cdot d\mathbf{r}$, where $\boldsymbol{A}(\boldsymbol{r}) = \frac{H}{2}(-y,x,0)$ stands for the vector potential with magnetic field H in the symmetric gauge and $\Phi_0 = hc/2e$ is the superconducting flux quantum. Within this choice of gauge, the next-nearest vortices of the square-vortex lattice are located at the 45° directions from the (100) direction. This vortex lattice configuration is suggested from the neutron-scattering experiment.[26,29,30] We have $t_{ij} = t_3$ and $t_{ij} = t_3'$ for the nearest-neighbor and next-nearest-neighbor hopping, respectively. The self-consistent equation for the pairing potential is reduced to

$$\Delta_{ij} = \frac{V}{2}\delta_{i,j\pm\hat{e}} \sum_\epsilon \left(u_j^\epsilon v_i^{\epsilon *} - v_j^{\epsilon *} u_i^\epsilon\right) \tanh\frac{E_\epsilon}{2T}, \tag{4}$$

with T being the temperature. Here, $\hat{e} = \hat{x},\hat{y}$, denoting the unit vector along the x and y direction, respectively. In this paper, we set $V = 1.0$.

The pair potential at each site i can be decomposed into p_x and p_y components as

$$\Delta_{p_x}(\boldsymbol{r}_i) = \frac{\Delta_{\hat{x},i} - \Delta_{-\hat{x},i}}{2}, \tag{5}$$

$$\Delta_{p_y}(\boldsymbol{r}_i) = \frac{\Delta_{\hat{y},i} - \Delta_{-\hat{y},i}}{2}. \tag{6}$$

Here we have denoted

$$\Delta_{\hat{e},i} = \Delta_{i,i+\hat{e}} \exp\left[i\frac{\pi}{\Phi_0}\int_{\boldsymbol{r}_i}^{\frac{\boldsymbol{r}_i+\boldsymbol{r}_{i+\hat{e}}}{2}} \boldsymbol{A}(\boldsymbol{r})\cdot \mathrm{d}\boldsymbol{r}\right]. \tag{7}$$

For $\sin p_x \pm i \sin p_y$-wave superconductivity, we can define the pairing potential as $\Delta_\pm(\boldsymbol{r}_i) \equiv \Delta_{p_x}(\boldsymbol{r}_i) \pm i\Delta_{p_y}(\boldsymbol{r}_i)$.

B. Quasi-1D model

We start with an effective two-orbital Hamiltonian that takes into account only the Ru d_{xz} and d_{yz} orbitals.[16,17,19] By assuming an effective attraction that causes the p-wave superconducting pairing, one can construct an effective model to study the vortex physics of the chiral p-wave superconductors in the mixed state. Here we ignore the on-site repulsion, which is not expected to change our conclusions qualitatively in the present problem.

After the mean-field decomposition, one arrives at the Bogoliubov-de Gennes equations

$$\sum_j \begin{pmatrix} H_{ij,mm} & \Delta_{ij,mm} & H_{ij,mn} & 0 \\ \Delta_{ij,mm}^\dagger & -H_{ij,mm}^* & 0 & -H_{ij,mn}^* \\ H_{ij,mn} & 0 & H_{ij,nn} & \Delta_{ij,nn} \\ 0 & -H_{ij,mn}^* & \Delta_{ij,nn}^\dagger & -H_{ij,nn}^* \end{pmatrix} \times \begin{pmatrix} u_{j,m}^\epsilon \\ v_{j,m}^\epsilon \\ u_{j,n}^\epsilon \\ v_{j,n}^\epsilon \end{pmatrix} = E_\epsilon \begin{pmatrix} u_{i,m}^\epsilon \\ v_{i,m}^\epsilon \\ u_{i,n}^\epsilon \\ v_{i,n}^\epsilon \end{pmatrix}, \tag{8}$$

where $H_{ij,\alpha\beta} = -e^{i\varphi_{ij}} t_{ij,\alpha\beta} - \delta_{ij}\delta_{\alpha\beta}\mu$, and $u_{j,m}^\epsilon$, $u_{j,n}^\epsilon$, $v_{j,m}^\epsilon$ and $v_{j,n}^\epsilon$ are the Bogoliubov quasiparticle amplitudes on the jth site with corresponding eigenvalues E_ϵ. Here, m and n denote the d_{xz} and d_{yz} orbitals, respectively. The hopping integrals are chosen as

$$t_{ij,\alpha\beta} = \begin{cases} t, & \alpha = \beta = m(n), \quad i = j \pm \hat{x}(\hat{y}) \\ -t', & \alpha \neq \beta, \quad i = j \pm (\hat{x}+\hat{y}) \\ t', & \alpha \neq \beta, \quad i = j \pm (\hat{x}-\hat{y}) \\ 0 & \text{otherwise.} \end{cases} \tag{9}$$

The matrix elements in the off-diagonal terms of Eq. (8) are obtained through the following self-consistent equations:

$$\begin{aligned} \Delta_{ij,mm} &= \frac{V}{2}\delta_{i,j\pm\hat{x}} \sum_\epsilon \left(u_{j,m}^\epsilon v_{i,m}^{\epsilon *} - v_{j,m}^{\epsilon *} u_{i,m}^\epsilon\right) \tanh\frac{E_\epsilon}{2T}, \\ \Delta_{ij,nn} &= \frac{V}{2}\delta_{i,j\pm\hat{y}} \sum_\epsilon \left(u_{j,n}^\epsilon v_{i,n}^{\epsilon *} - v_{j,n}^{\epsilon *} u_{i,n}^\epsilon\right) \tanh\frac{E_\epsilon}{2T}. \end{aligned} \tag{10}$$

The orbital part of the order parameter can be decomposed as

$$\Delta_{p_x}(\boldsymbol{r}_i) = \frac{\Delta_{\hat{x},i} - \Delta_{-\hat{x},i}}{2}, \tag{11}$$

$$\Delta_{p_y}(\boldsymbol{r}_i) = \frac{\Delta_{\hat{y},i} - \Delta_{-\hat{y},i}}{2}, \tag{12}$$

where we denote

$$\begin{aligned} \Delta_{\hat{x},i} &= \Delta_{i,i+\hat{x},mm} \exp\left[i\frac{\pi}{\Phi_0}\int_{\boldsymbol{r}_i}^{\frac{\boldsymbol{r}_i+\boldsymbol{r}_{i+\hat{x}}}{2}} \boldsymbol{A}(\boldsymbol{r})\cdot \mathrm{d}\boldsymbol{r}\right], \\ \Delta_{\hat{y},i} &= \Delta_{i,i+\hat{y},nn} \exp\left[i\frac{\pi}{\Phi_0}\int_{\boldsymbol{r}_i}^{\frac{\boldsymbol{r}_i+\boldsymbol{r}_{i+\hat{y}}}{2}} \boldsymbol{A}(\boldsymbol{r})\cdot \mathrm{d}\boldsymbol{r}\right]. \end{aligned} \tag{13}$$

For $\sin p_x \pm i \sin p_y$-wave superconductivity,[31] we can define the pairing potential as

$$\Delta_{\pm}(\boldsymbol{r}_i) \equiv \Delta_{p_x}(\boldsymbol{r}_i) \pm i\Delta_{p_y}(\boldsymbol{r}_i). \tag{14}$$

Without loss of generality, we restrict the calculations with Δ_+ and Δ_- as the major and minor components of the order parameters. Two types of vortices arise, depending on the direction of the magnetic field insofar as the chirality is fixed.[32] In numerical computations, the unit cell with size $N_x \times N_y = 33 \times 33$ and the number of such magnetic unit cells $M_x \times M_y = 5 \times 5$ are used.[33]

C. Calculation of experimental observables

In this section, we discuss the formalism for the local density of states (LDOS) and the nuclear spin-lattice relaxation rate in both models for Sr_2RuO_4. In the scanning tunneling microscope (STM) experiment, the tunneling conductance is proportional to the LDOS $N(E,\mathbf{r}_i)$, which can be calculated as

$$N(E,\mathbf{r}_i) = -\sum_{\epsilon}\left[\left|\mathcal{U}_i^{\epsilon}\right|^2 f'(E_\epsilon - E) + \left|\mathcal{V}_i^{\epsilon}\right|^2 f'(E_\epsilon + E)\right], \tag{15}$$

where $f'(E)$ is the derivative of the Fermi-Dirac distribution function with respect to energy. Hereafter we denote

$$\mathcal{U}_i^{\epsilon} = u_i^{\epsilon}, \quad \mathcal{V}_i^{\epsilon} = v_i^{\epsilon} \tag{16}$$

for the single-band model, and

$$\mathcal{U}_i^{\epsilon} = u_{i,m}^{\epsilon} + u_{i,n}^{\epsilon}, \quad \mathcal{V}_i^{\epsilon} = v_{i,m}^{\epsilon} + v_{i,n}^{\epsilon} \tag{17}$$

for the quasi-1D model.

In addition to the STM measurement, nuclear magnetic resonance (NMR) or nuclear quadrupole resonance (NQR) is another related powerful method to identify distinct signatures predicted by different models. Generally speaking, this method is able to simultaneously shed light on the spatial profile of the zero-energy quasiparticles through the relaxation time T_1. The nuclear spin-lattice relaxation rate we consider is given by[34,35]

$$\begin{aligned} R(r_i,r_{i'}) &= \mathrm{Im}\chi_{+,-}(r_i,r_{i'},i\Omega_n \to \Omega + i\eta)/(\Omega/T)|_{\Omega\to 0} \\ &= -\sum_{\epsilon,\epsilon'} \mathcal{U}_i^{\epsilon}\mathcal{U}_i^{\epsilon'*}\left[\mathcal{U}_{i'}^{\epsilon}\mathcal{U}_{i'}^{\epsilon'*} + \mathcal{V}_{i'}^{\epsilon}\mathcal{V}_{i'}^{\epsilon'*}\right] \\ &\quad \times \pi T f'(E_\epsilon)\delta(E_\epsilon - E_{\epsilon'}). \end{aligned} \tag{18}$$

We choose $\mathbf{r}_i = \mathbf{r}_{i'}$ by considering that the nuclear spin-lattice relaxation at a local site is dominant. Then the site-dependent relaxation time is given by $T_1(r) = 1/R(r,r)$. Roughly speaking, T_1 is proportional to the integral of the LDOS within the energy range $0 \leqslant E \leqslant T$. Therefore, the NMR/NQR experiment is also expected to provide important fingerprints for the two models.

IV. RESULTS

In this section, we will present results for the vortex states based on the two different models and basic methods discussed in the previous section.

A. Vortex structure

To begin with, a general picture of the vortex structure for the superconducting order parameters for both models will be shown below. We will also show the spatial dependence of the pairing order parameter and LDOS at zero bias. While the former cannot be measured directly, the LDOS is an experimentally observable quantity in the STM measurement.

First, we study the single-band model and plot the order parameters as a function of position in a vortex lattice in Fig. 3. Due to the broken time-reversal symmetry of the chiral p-wave state, there are two types of vortices depending on the direction of the magnetic field. However, the negative vortex with winding number opposite to the chirality is the stable state.[36] And as shown in Fig. 3, the orientation of the square shape is different depending on the winding. In the negative or positive vortex case, the shape of $|\Delta_+|$ around the vortex core is nearly isotropic with minor anisotropy. However, the induced component $|\Delta_-|$ in both negative and positive vortex shows similar shapes, which extends along the a axis. Finally, as shown in Figs. 3(e) and 3(f), we also calculate the LDOS $N(E=0,\boldsymbol{r})$, which is related to the tunneling conductance at zero bias in the STM experiment. We can see that the LDOS comes to a peak around the vortex core, with slightly anisotropic extension along the (110) direction. This is because the amplitude of Fermi velocity v_F for the γ band is almost isotropic with slight enhancement near the (110) direction, as shown in Fig. 2(b). Such features are qualitatively similar to previous results.[26]

Now we turn to the results for the quasi-1D model. Similar calculations to the single-band case are performed, with the corresponding results shown in Fig. 4. We find several qualitative differences resulting from the different models after careful comparison. First, in this model, the amplitude of the major component $\Delta_+(\boldsymbol{r})$ is not substantially suppressed at the vortex core, compared with the previous model. This can be seen from the density scale of Figs. 4(a) and 4(b), showing a variation from about 0.3 to 0.6, whereas the counterpart for the single-band model in Figs. 3(a) and 3(b) is from 0.1 to 0.5. Second, for the induced component $\Delta_-(\boldsymbol{r})$, its amplitude reaches a maximum at the vortex core. On the contrary, $|\Delta_-(\boldsymbol{r})|$ maximizes near the core along the a or b axis and shows a fourfold symmetry.

More importantly, one should pay attention to the LDOS at zero bias for this model. At a first glance, the shape of the LDOS around the vortex resembles a rhombus ($\diamond$), with its vertices pointing along the a or b axis. Such a highly anisotropic structure is actually an indication of strong anisotropy for the angle-resolved Fermi velocity. This intuitive understanding is supported by our calculations showing that $|\vec{v}_F|$ in the normal state is maximized along the a or b axis for both α and β bands in Fig. 2(b). As a result, the shape of the LDOS at zero bias, acting as a fingerprint of the active band where the superconductivity arises, can be used to distinguish the two different models in the STM measurement.

Moreover, we find that the peak feature at the vortex core is substantially smeared for the quasi-1D model [pay attention to the density scale of Figs. 4(e) and 4(f) in comparison with the single-band counterpart in Figs. 3(e) and 3(f)]. This property is unique for a quasi-1D model,[37] and the underlying physics is

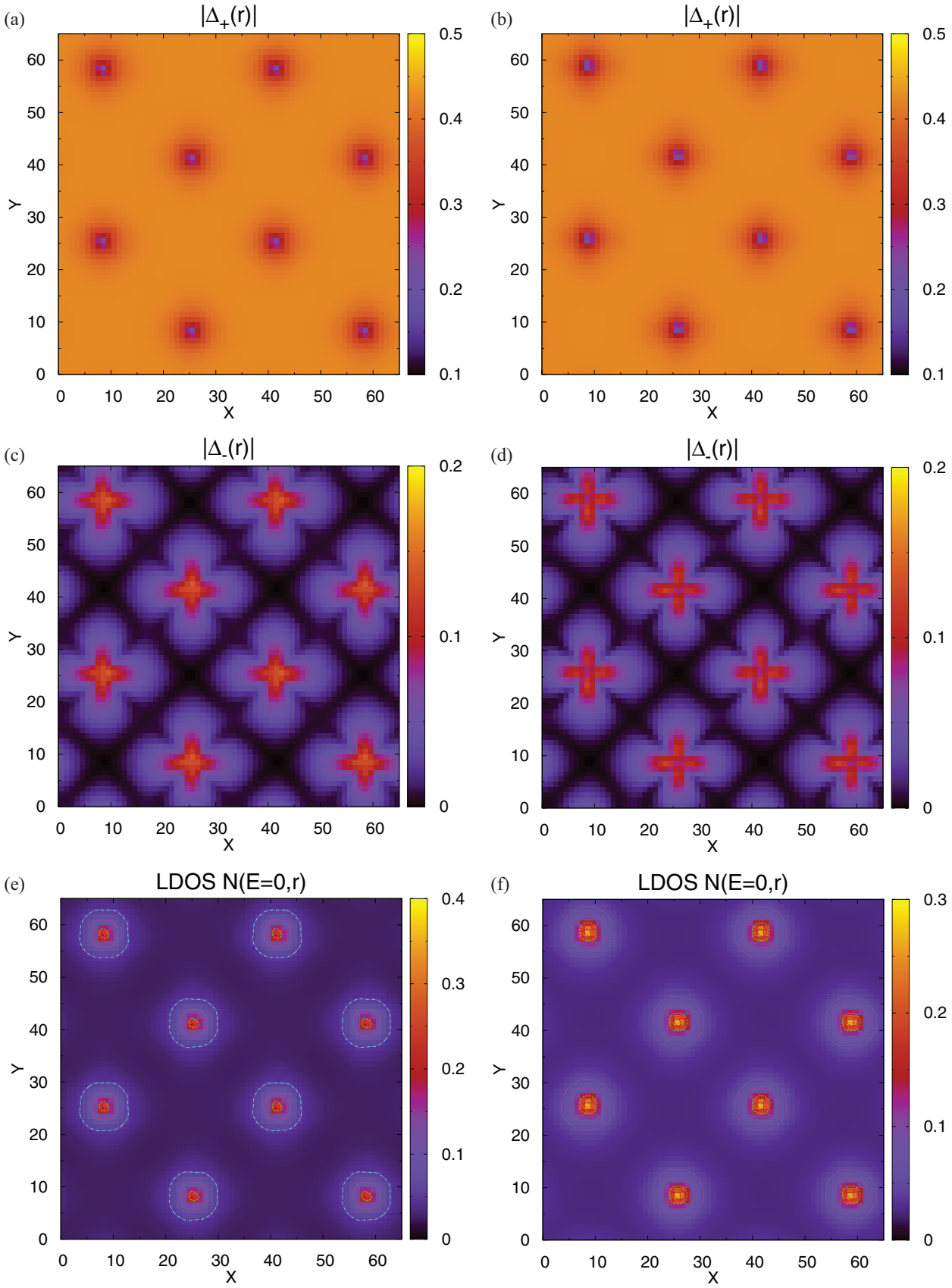

FIG. 3. (Color online) Vortex lattice structure in a single-band model. Left panels are for a negative vortex lattice and right panels are for a positive vortex lattice. (a), (b): spatial distribution of the major component $|\Delta_+(\boldsymbol{r})|$; (c), (d): spatial distribution of the admixed component $|\Delta_-(\boldsymbol{r})|$; (e), (f): LDOS at zero bias $N(E=0,\boldsymbol{r})$. The size of a magnetic unit cell is 33×33.

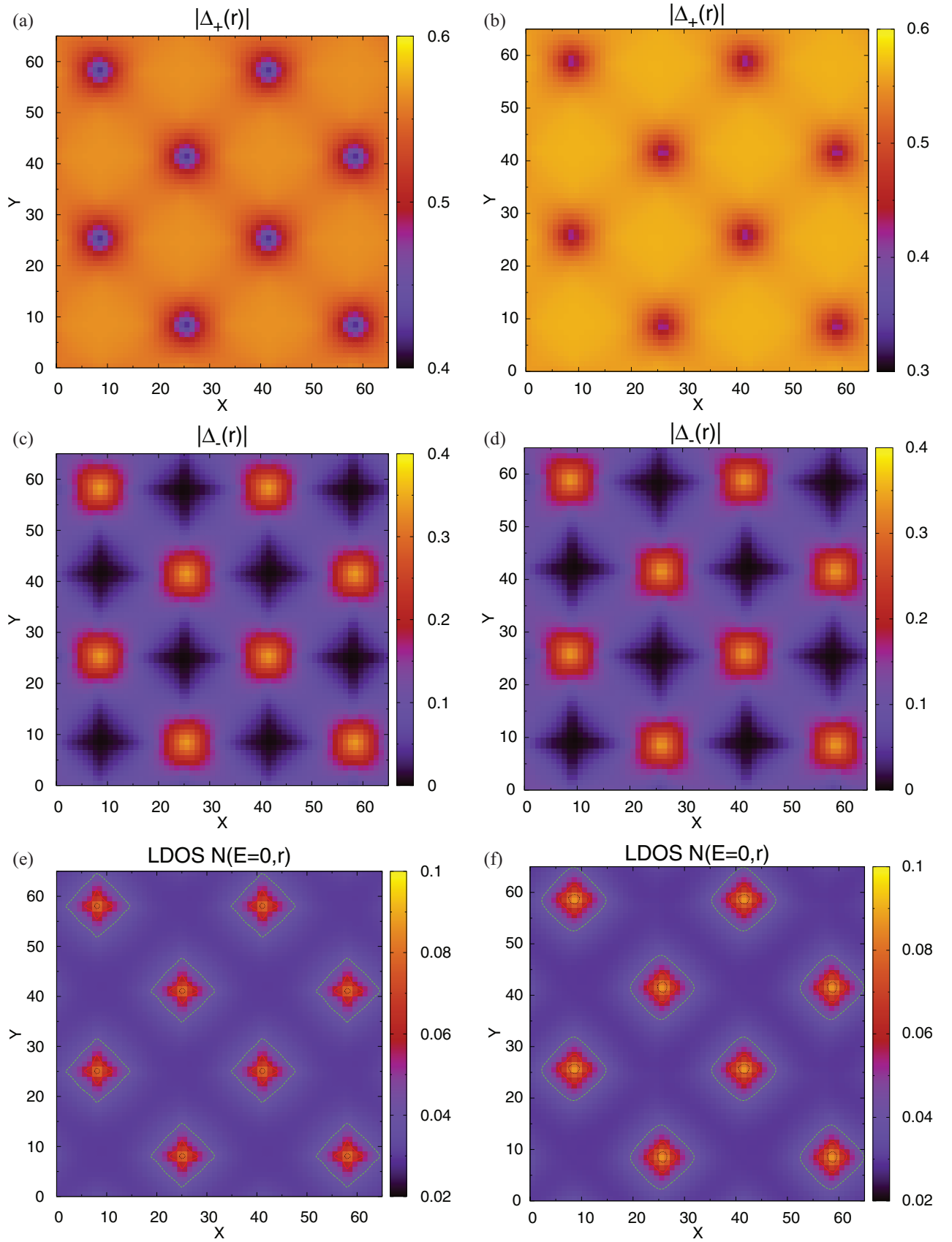

FIG. 4. (Color online) Vortex lattice structure in a two-band model. Left panels are for a negative vortex lattice and right panels are for a positive vortex lattice. (a), (b): spatial distribution of the major component $|\Delta_+(\boldsymbol{r})|$; (c), (d): spatial distribution of the admixed component $|\Delta_-(\boldsymbol{r})|$; (e), (f): LDOS at zero bias $N(E=0,\boldsymbol{r})$. The size of a magnetic unit cell is 33×33.

the strong suppression of low-energy resonance in the vortex state of a quasi-1D model, which will be discussed in detail with more experimental signatures below.

B. Signatures in STM and NMR/NQR measurements

After giving a general perspective of the vortex structure for the two different models, below we would like to study and analyze the LDOS in detail. The energy dependence of LDOS can be directly probed by measuring the tunneling conductance with an appropriate voltage bias in the STM experiment. In Fig. 5, we show a comparison of the energy-resolved LDOS at various positions for the two models. In the single-band model, we can see that the LDOS at the core of the negative vortex has a peak at $E=0$, while the peak for the positive vortex is slightly higher than zero. This feature, qualitatively consistent with previous calculations, is due to different winding structures of the negative and positive vortices.[26]

However, the situation is totally different in the quasi-1D model. Similar study on organic superconductors in a magnetic field[37] indicates that vortices are strongly modified due to the quasi-1D nature of superconductivity. Specifically, it has been demonstrated that vortices in a quasi-1D superconductor do not possess low-energy midgap excitations. This extraordinary property leads to the missing of midgap resonance peak in the energy dependence of LDOS at the vortex site. To see whether or not this conclusion can be applied to our quasi-1D model for Sr_2RuO_4, we also calculate the energy dependence of the LDOS at different positions in Fig. 5(b). It can be seen that the midgap resonance is also absent in the quasi-1D model we consider here. Nevertheless, we want to stress that this conclusion is valid only when the interorbital hopping amplitude t' is small enough. On the contrary, if t' is large enough, say $t'>0.4t$, we find that the midgap resonance will be present again, similar to the single-band model.

Not only does the STM technique enable direct detection of the midgap excitations at the vortex core, but these excitations are also expected to be indicated in the NMR/NQR experiment. Now, we proceed to the discussion of the nuclear spin-lattice relaxation rate T_1^{-1}, which can be calculated via Eq. (18). For the single-band model, from Fig. 6(a) we can see that a residual relaxation rate shows up at the vortex core as the

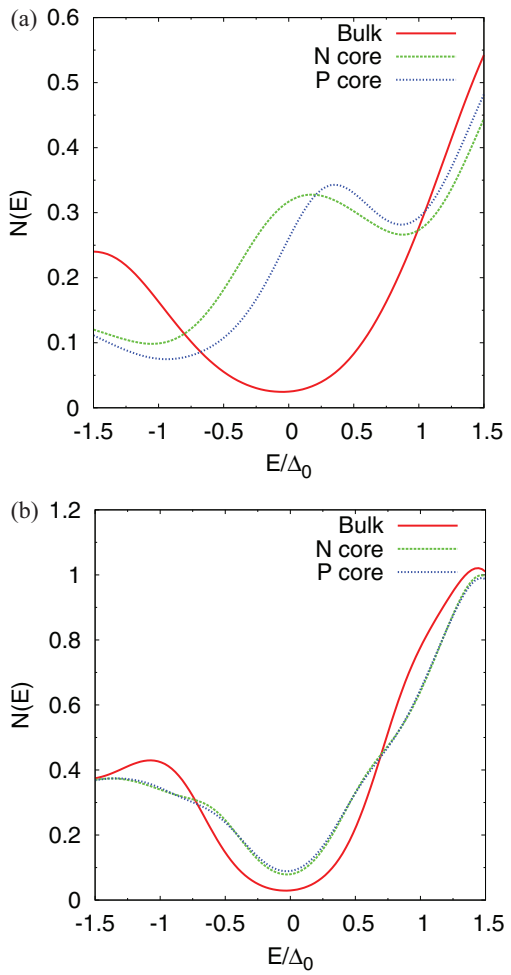

FIG. 5. (Color online) LDOS $N(E,\boldsymbol{r})$ as a function of energy E at various positions for (a) the single-band model and (b) quasi-1D model. The bulk value is obtained in the absence of a magnetic field, whereas "N core" ("P core") indicates the position at the negative (positive) vortex core. The temperature is about $0.3T_c$.

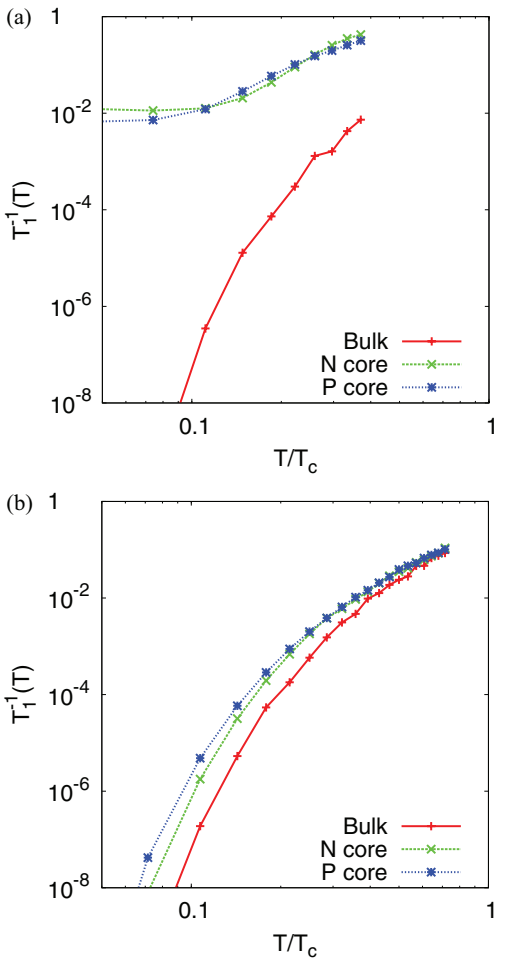

FIG. 6. (Color online) The nuclear spin-lattice relaxation rate T_1^{-1} as a function of temperature T at various positions for (a) a single-band model and (b) a quasi-1D model. The bulk value is obtained in the absence of a magnetic field, whereas "N core" ("P core") indicates the position at the negative (positive) vortex core.

temperature approaches zero, making T_1^{-1} deviate from the bulk value by several orders of magnitude especially at low temperatures, consistent with previous calculations.[38] This huge deviation stems from the fact that the midgap states of the vortex core contribute substantially to the relaxation rate, compared to the zero-field case. Next, we turn to the quasi-1D scenario in Fig. 6(b). Note that the temperature dependence of the relaxation rate at different positions is almost identical in the logarithmic scale. The only subtle difference between the bulk and the vortex core is that T_1^{-1} is slightly enhanced at low temperatures in the vortex core, but the previous residual behavior is totally absent. This result is consistent with the previous discussions on the energy dependence of LDOS, which also show similar behaviors between the bulk and the vortex core.

Although the measurement of the nuclear spin-lattice relaxation rate turns out to be a promising experiment to identify the active source of superconductivity in Sr_2RuO_4, several minor comments are unavoidable. First, contributions to the relaxation rate from various positions of vortex cores usually cannot be separated clearly in experiments. Therefore, comparison experiments in the presence and absence of vortices need to be carried out carefully. Second, as mentioned previously, all of the bands participate in pairing at very low T due to interband proximity effects.[7] Therefore, measurements should be performed at T well above zero, say $0.1T_c < T < T_c$. In the temperature range, a salient distinction is still expected, as illustrated in Fig. 6.

For Sr_2RuO_4, the spin-lattice relaxation rate has been measured by the NQR technique in the absence of a magnetic field down to 0.1 K.[39] And we suggest that further experiments in an external field should be performed as a crucial test of the two candidate models, in spite of some minor difficulties discussed above.

V. SUMMARY AND CONCLUSION

We have studied the vortex state for a chiral p-wave superconductor based on a single 2D band and two quasi-1D band models, respectively. By comparing the two sets of results, we have found several distinctive characteristics in the vortex state derived from different models. Generally speaking, for the band structure of Sr_2RuO_4 at the Fermi surface, the γ band is more or less isotropic in the x-y plane, whereas the quasi-1D α and β bands are highly anisotropic. Assuming that superconductivity originates from either the γ band or α and β bands, the vortex state does inherit distinguishable features from the active band(s). First, the shape of the LDOS at zero bias in the quasi-1D model shows anisotropy in accordance with the analysis of the angle-resolved Fermi velocity for the α and β bands. Second, the missing of the midgap resonance at the vortex core for this model leads to corresponding consequences in the energy dependence of LDOS and the temperature dependence of nuclear spin-lattice relaxation rate T_1^{-1}. All of these specialities show a sharp distinction compared with the counterparts in the single-band scenario. Consequently, the STM and NMR/NQR measurements in the vortex state of Sr_2RuO_4 are expected to be unambiguous experiments to answer the question of which band the superconductivity resides in. Before concluding, we would like to mention that it has been recently proposed that this disputatious issue related to the orbital origin of superconductivity can be settled by detecting the Leggett-like collective modes.[40]

ACKNOWLEDGMENTS

We thank T. M. Rice for discussion. This work is partly supported by HK RGC GRF Grant No. HKU10 and by NSFC Grant No. J20121499.

[1] A. P. Mackenzie and Y. Maeno, Rev. Mod. Phys. **75**, 657 (2003).
[2] Y. Maeno, H. Hashimoto, K. Yoshida, S. Nishizaki, T. Fujita, J. G. Bednorz, and F. Lichtenberg, Nature (London) **372**, 532 (1994).
[3] T. Rice and M. Sigrist, J. Phys.: Condens. Matter **7**, L643 (1995).
[4] G. Baskaran, Physica B **223**, 490 (1996).
[5] K. Miyake and O. Narikiyo, Phys. Rev. Lett. **83**, 1423 (1999).
[6] K. Deguchi, Z. Q. Mao, and Y. Maeno, J. Phys. Soc. Jpn. **73**, 1313 (2004).
[7] D. F. Agterberg, T. M. Rice, and M. Sigrist, Phys. Rev. Lett. **78**, 3374 (1997).
[8] K. Deguchi, Z. Q. Mao, H. Yaguchi, and Y. Maeno, Phys. Rev. Lett. **92**, 047002 (2004).
[9] A. P. Mackenzie, S. R. Julian, A. J. Diver, G. J. McMullan, M. P. Ray, G. G. Lonzarich, Y. Maeno, S. Nishizaki, and T. Fujita, Phys. Rev. Lett. **76**, 3786 (1996).
[10] C. Kallin, Rep. Prog. Phys. **75**, 042501 (2012).
[11] Y. Maeno, S. Kittaka, T. Nomura, S. Yonezawa, and K. Ishida, J. Phys. Soc. Jpn. **81**, 011009 (2012).
[12] K. Sengupta, H.-J. Kwon, and V. M. Yakovenko, Phys. Rev. B **65**, 104504 (2002).
[13] K. Sengupta and V. M. Yakovenko, Phys. Rev. Lett. **101**, 187003 (2008).
[14] P. G. Björnsson, Y. Maeno, M. E. Huber, and K. A. Moler, Phys. Rev. B **72**, 012504 (2005).
[15] J. R. Kirtley, C. Kallin, C. W. Hicks, E.-A. Kim, Y. Liu, K. A. Moler, Y. Maeno, and K. D. Nelson, Phys. Rev. B **76**, 014526 (2007).
[16] S. Raghu, A. Kapitulnik, and S. A. Kivelson, Phys. Rev. Lett. **105**, 136401 (2010).
[17] Y. Imai, K. Wakabayashi, and M. Sigrist, Phys. Rev. B **85**, 174532 (2012).
[18] S. Raghu, S. B. Chung, and S. Lederer, arXiv:1208.6344.
[19] E. Taylor and C. Kallin, Phys. Rev. Lett. **108**, 157001 (2012).
[20] K. I. Wysokiński, J. F. Annett, and B. L. Györffy, Phys. Rev. Lett. **108**, 077004 (2012).
[21] V. M. Yakovenko, Phys. Rev. Lett. **98**, 087003 (2007).
[22] J. Xia, Y. Maeno, P. T. Beyersdorf, M. M. Fejer, and A. Kapitulnik, Phys. Rev. Lett. **97**, 167002 (2006).
[23] J. Huo, T. M. Rice, and F.-C. Zhang, arXiv:1301.2865.
[24] M. Braden, Y. Sidis, P. Bourges, P. Pfeuty, J. Kulda, Z. Mao, and Y. Maeno, Phys. Rev. B **66**, 064522 (2002).
[25] A. Damascelli, Z. Hussain, and Z.-X. Shen, Rev. Mod. Phys. **75**, 473 (2003).
[26] M. Takigawa, M. Ichioka, K. Machida, and M. Sigrist, Phys. Rev. B **65**, 014508 (2001).

[27]H. Kontani, T. Tanaka, D. S. Hirashima, K. Yamada, and J. Inoue, Phys. Rev. Lett. **100**, 096601 (2008).

[28]A. Damascelli, D. H. Lu, K. M. Shen, N. P. Armitage, F. Ronning, D. L. Feng, C. Kim, Z.-X. Shen, T. Kimura, Y. Tokura, Z. Q. Mao, and Y. Maeno, Phys. Rev. Lett. **85**, 5194 (2000).

[29]T. M. Riseman, P. G. Kealey, E. M. Forgan, A. P. MacKenzie, L. M. Galvin, A. W. Tyler, S. L. Lee, C. Ager, D. M. Paul, C. M. Aegerter, R. Cubitt, Z. Q. Mao, T. Akima, and Y. Maeno, Nature (London) **396**, 242 (1998).

[30]P. G. Kealey, T. M. Riseman, E. M. Forgan, L. M. Galvin, A. P. Mackenzie, S. L. Lee, D. M. Paul, R. Cubitt, D. F. Agterberg, R. Heeb, Z. Q. Mao, and Y. Maeno, Phys. Rev. Lett. **84**, 6094 (2000).

[31]It has been proposed that the order parameter in the quasi-1D model should assume a slightly different form, namely, $\sin p_x \cos p_y \pm i \sin p_y \cos p_x$.[16] Nevertheless, we believe that most of our conclusions can be qualitatively applied to this case too.

[32]M. Matsumoto and R. Heeb, Phys. Rev. B **65**, 014504 (2001).

[33]Y. Wang and A. H. MacDonald, Phys. Rev. B **52**, R3876 (1995).

[34]M. Takigawa, M. Ichioka, and K. Machida, Phys. Rev. Lett. **83**, 3057 (1999).

[35]H.-M. Jiang, J. Guo, and J.-X. Li, Phys. Rev. B **84**, 014533 (2011).

[36]R. Heeb and D. F. Agterberg, Phys. Rev. B **59**, 7076 (1999).

[37]M. Takigawa, M. Ichioka, K. Kuroki, Y. Asano, and Y. Tanaka, Phys. Rev. Lett. **97**, 187002 (2006).

[38]M. Takigawa, M. Ichioka, K. Machida, and M. Sigrist, J. Phys. Chem. Sol. **63**, 1333 (2002).

[39]K. Ishida, H. Mukuda, Y. Kitaoka, Z. Q. Mao, Y. Mori, and Y. Maeno, Phys. Rev. Lett. **84**, 5387 (2000).

[40]S. B. Chung, S. Raghu, A. Kapitulnik, and S. A. Kivelson, Phys. Rev. B **86**, 064525 (2012).